

1 **Volumetric solid concentration as a main proxy for basal force fluctuations generated**
2 **by highly concentrated sediment flows**

3
4 **M. Piantini^{1,2}, F. Gimbert¹, E. Korkolis¹, R. Rousseau², H. Bellot² and A. Recking²**

5 ¹University Grenoble Alpes, CNRS, IRD, Institute for Geosciences and Environmental Research
6 (IGE), Grenoble, France.

7 ²University Grenoble Alpes, INRAE, ETNA, Grenoble, France.
8

9 Corresponding author: Marco Piantini (marco.piantini@tiscali.it)

10 **Key Points:**

- 11 • We investigate the seismic signature of laboratory highly concentrated flows exhibiting
12 rheological stratification and grain sorting
- 13 • We observe a negative relationship between the volumetric solid concentration and the
14 amplitude of basal force fluctuations
- 15 • We suggest volumetric solid concentration should be incorporated in seismic models as a
16 key parameter describing particle agitation
17

18 **Abstract**

19 Sediment flows generate ground vibrations by exerting basal force fluctuations on the riverbed,
20 which motivates the use of seismology to indirectly measure flow properties. Linking the force
21 fluctuations and properties of highly concentrated sediment flows, however, remains particularly
22 challenging due to complexities that arise from grain-to-grain interactions. Here we conduct
23 downscaled flume experiments designed to investigate the influence of grain scale processes on
24 the generation of force fluctuations for stratified sediment flows associated with significant grain
25 sorting. We demonstrate that, under such flow conditions, the amplitude of force fluctuations
26 decreases as the volumetric solid concentration increases. We suggest that this dependency
27 reflects the negative relationship between volumetric solid concentration and particle agitation,
28 which in turn controls the amplitude of force fluctuations. We therefore advance that volumetric
29 solid should be incorporated in seismic models as a key parameter describing the particle
30 agitation of highly concentrated sediment flows.

31 **Plain Language Summary**

32 Flowing through the landscape, a wide range of fluvial processes generate high-frequency
33 ground vibrations (> 1 Hz) by exerting force fluctuations on the bed. This evidence has
34 motivated the use of seismology to indirectly measure sediment transport properties, such as the
35 diameter of the transported sediments, the flux, the thickness and velocity of sediment flows.
36 However, it is still particularly challenging to link the force fluctuations and properties of highly
37 concentrated sediment due to complexities that arise from grain scale processes. Here we focus
38 our attention on grain sorting and rheological stratification, which are quite common in such
39 sediment flows but whose effect on force fluctuations has rarely been investigated. To do so we
40 conduct downscaled flume experiments designed to reproduce highly concentrated flows
41 characterized by a wide bimodal grain size distribution typical of mountain streams. We identify
42 the volumetric solid concentration as the key parameter describing the amplitude of basal force
43 fluctuations through its unique link with the flow particle agitation. This finding offers new
44 insights for the interpretation of the force fluctuations generated by highly concentrated flows
45 and underline limits of current theoretical models.

46 **1 Introduction**

47 Flowing through the landscape, rivers generate high-frequency ground vibrations (> 1
48 Hz) by exerting force fluctuations on their bed (Burtin et al., 2016; Larose et al., 2015). There is
49 well-established evidence that seismic sensors detect ground vibrations from a wide variety of
50 fluvial sediment transport events including very energetic ones (Arattano & Moia, 1999; Burtin
51 et al., 2016; Cook et al., 2018, 2021; Govi et al., 1993; McCoy et al., 2013), calling for
52 seismology as an appealing way to remotely monitor sediment transport characteristics and
53 processes.

54 Through laboratory experiments and field observations, numerous efforts have recently
55 been dedicated to investigate the relationships between the amplitude of force fluctuations and
56 the properties of various sediment flows, ranging from bedload to debris flows (Allstadt et al.,
57 2020; Bakker et al., 2020; Cole et al., 2009; Coviello et al., 2018, 2019; Gimbert et al., 2019;
58 Haas et al., 2021; Hsu et al., 2014; McCoy et al., 2013; Zhang, Walter, McArdell, Haas, et al.,
59 2021). In parallel, physically-based mechanistic models have been developed to establish
60 quantitative links between flow properties and the seismic signal (Tsai et al., 2012; Gimbert et

61 al., 2019; Bachelet et al., 2021; Farin et al., 2019; Lai et al., 2018; Zhang, Walter, McArdell,
62 Haas, et al., 2021). Models concerning bedload transport predict that sediment flux and
63 transported grain sizes are major control parameters, the former mainly setting the rate of
64 impacts and the latter the impact-released energy. These theoretical expectations have been
65 verified through experiments and field observations under relatively low bedload transport rates
66 (Bakker et al., 2020; Gimbert et al., 2019; Lagarde et al., 2021; Roth et al., 2016).

67 However, more complexity arises when dealing with highly concentrated sediment flows,
68 for which existing observations reveal not straightforward relationships between flow properties
69 and the amplitude of force fluctuations. Coarse granular and debris flows have been shown to
70 generate stronger force fluctuations compared to finer ones (Haas et al., 2021; Hsu et al., 2014;
71 Zhang, Walter, McArdell, Haas, et al., 2021), but the presence of big particles does not
72 necessarily correspond to high force fluctuations, likely depending on their position relative to
73 the bed (Piantini et al., 2021; Zhang, Walter, McArdell, Haas, et al., 2021). Certain
74 investigations show amplitudes of force fluctuations that are positively correlated with flow
75 thickness and mass (McCoy et al., 2013; Zhang, Walter, McArdell, Haas, et al., 2021), others
76 report poorer correlations when bulk density varies fast (Allstadt et al., 2020), or even negative
77 correlations in the case of mud-saturated debris flows (Hsu et al., 2014). Hsu et al. (2014)
78 illustrate that sediment flow velocity exerts a primary control on force fluctuations, while
79 Allstadt et al. (2020) and Zhang et al. (2021) observe a rather low correlation.

80 These complex and sometimes contrasting observations suggest the need to investigate
81 more deeply the control of grain scale processes on the generation of force fluctuations (Allstadt
82 et al., 2020). Grain sorting processes (Frey & Church, 2009; Iverson et al., 2010; Johnson et al.,
83 2012) and rheological flow stratification, intended as the occurrence of significant variations of
84 flow rheology over depth (Armanini et al., 2005; GDR MiDi, 2004; Manville & White, 2003; Y.
85 K. Sohn, 1997), may play a role as they influence the distribution of grain sizes and reflect the
86 degree of particle agitation (GDR MiDi, 2004; Iverson et al., 1997; Y. K. Sohn, 1997),
87 respectively. However, these mechanisms have been rarely taken into account for interpreting
88 observations or investigated in experimental works, and are typically neglected in theoretical
89 models (Bachelet et al., 2021; Farin et al., 2019; Lai et al., 2018; Zhang, Walter, McArdell, Haas,
90 et al., 2021). It thus remains unclear to which extent the above-mentioned processes may control
91 the generation of force fluctuations, and whether such control may be described as a function of
92 bulk flow properties.

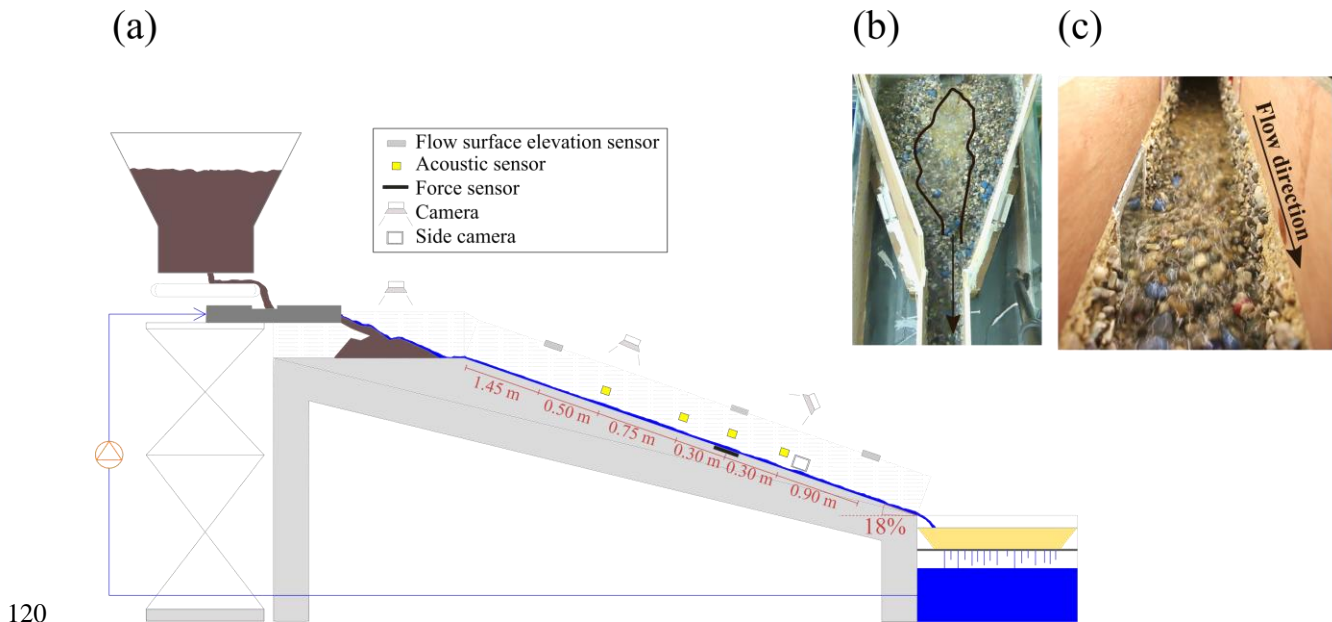
93 In order to address this lack, here we conduct downscaled flume experiments designed to
94 reproduce self-triggered highly concentrated flows characterized by a wide bimodal grain size
95 distribution typical of mountain streams, and experiencing significant rheological flow
96 stratification and grain sorting. We investigate their propagation in a steep rough channel while
97 independently measuring flow properties and its seismic signature. We identify the volumetric
98 solid concentration as the key parameter describing the amplitude of basal force fluctuations
99 through its unique link with the flow particle agitation.

100 **2 Methods**

101 2.1 Experimental setup and conditions

102 We carry out laboratory experiments in a flume composed of a 5-m long and 0.1-m wide
103 straight steep channel (slope of 18%), connected in its upstream part to a 1-m long and on

104 average 0.5-m wide storage area (slope of 0 – 1%) (Figure 1a-b). Every run consists in feeding
 105 the upstream storage area with constant liquid discharge Q_l ($Q_l \in [0.48; 0.55 \text{ l/s}]$) and sediment
 106 flux Q_s ($Q_s \in [70; 100 \text{ g/s}]$) whose values are based on similitude criteria to reproduce typical
 107 supercritical and fully turbulent flood conditions in mountain rivers (Piantini et al., 2021). We
 108 use a bimodal grain size distribution typical of mountain rivers (Casagli et al., 2003; John
 109 Wolcott, 1988; Sklar et al., 2017). The sediment size mixture is characterized by two modes
 110 corresponding to sand ($0.5 \text{ mm} < D < 2 \text{ mm}$) and cobbles ($4 \text{ mm} < D < 8 \text{ mm}$) (see Figure 4 in
 111 (Piantini et al., 2021)), with $D_{50} = 5.16 \text{ mm}$ and $D_{84} = 9 \text{ mm}$. The bed and side walls of the
 112 flume are covered with sediments taken by the same sediment mixture and fixed with silicone.
 113 The sediment deposit that forms in the storage area is subject to alternating stages of aggradation
 114 and erosion (Figure 1a), with every erosion phases generating sediment pulses that propagate in
 115 the downstream steep channel (Figure 1b). Here we investigate specifically sediment pulses. We
 116 have investigated 4 sediment pulses in total, two of them are presented in the main text (hereafter
 117 referred to as Exp #1 and Exp #2) and the others in the Supporting Information. All the flow
 118 properties presented and discussed in the following sections are averaged over these two
 119 experiments.



120

121 **Figure 1.** (a) Sketch of the experimental flume. (b) Frame taken from the video recording of the
 122 storage area during an experiment. The area interested by the erosion phase is circled in black.
 123 (c) Frame taken from the video recording over the force sensor during an experiment.

124 2.2 Instrumentation

125 Seismically relevant quantities are measured through seismic and force sensors. Four
 126 Glaser-type KRNBB-PC piezoelectric sensors, which we here refer to as seismic sensors, are
 127 mounted on the outside of one of the sidewalls of the channel, using mounting brackets and
 128 double-sided adhesive tape (Figure 1a and Figure S1). The sensors are connected via an AMP-
 129 12BB-J preamplifier to an Elexis Spectrum digitizer with sampling frequency f_s set to 200 kHz.
 130 The mean basal force and force fluctuations are measured by coupling a 0.07-m wide and 0.1-m
 131 long rectangular steel plate onto the channel bed with two piezoelectric force sensors (model

132 Kistler Typ 9601A21 connected to a Kistler 5073 charge amplifier) measuring the normal and
 133 downslope forces exerted by the flow on the plate (using $f_s = 30$ kHz). The plate is
 134 mechanically isolated from the rest of the flume to minimize its sensitivity to flume vibrations,
 135 and is covered by sediments fixed with silicone (Supporting Information).

136 We also monitor several in-stream flow properties simultaneously. We measure the flow
 137 surface elevation in three different sections of the channel (Figure 1a) by means of three
 138 ultrasonic sensors (Banner Q45UR Series, using $f_s = 100$ Hz). We sample and sieve the
 139 sediment flux by hand at the flume outlet with a frequency of about 1 sample / 5 sec. We
 140 estimate the volumetric solid concentration by evaluating the bulk density as the ratio between
 141 the mean normal stress and the flow surface elevation (Iverson et al., 2010). We also estimate the
 142 macroscopic velocity of the sediment flows (U_x) and the downstream velocity of the biggest
 143 particles (u_x) by combining multiple sets of observations (Supporting Information). We video
 144 record each experiment through a camera (Canon EOS 200D) and a webcam (Microsoft HD
 145 LifeCam Cinema) in the upstream and downstream parts of the flume, respectively (Figure 1a).
 146 The upstream camera is installed perpendicular to the channel bed and covers a stretch of 0.30
 147 m, while the webcam is inclined to allow a wider look on the channel length (Figure 1c).

148 2.3 Seismic and force data processing

149 We analyse the seismic and normal force fluctuation time series through computing the
 150 power spectral density (PSD) using Welch's averaging method (Welch, 1967). Time series are
 151 split into 50% overlapping segments of 0.5 s for the seismic signal and 1 s for the force signal.
 152 Force power and flow property time series are smoothed using a 5-s moving window. We
 153 consider the frequency range 100 – 2500 Hz to avoid dealing with strong plate resonances and
 154 the contribution of impacts on the side walls, which are particularly noticeable above 2500 Hz
 155 (Figure S2), and to limit the contribution of water flow to the seismic noise (e.g. water pump,
 156 water flow in pipes and on the flume), which is significant below 100 Hz (Piantini et al., 2021).

157 3 Results

158 3.1 General observations

159 3.1.1 In-stream transport dynamics

160 The self-triggered destabilizations of the upstream sediment deposit generate a
 161 downstream propagating pulse made of three distinct sediment transport phases exhibiting
 162 different dynamics and grain size compositions:

163 - Phase I (“Front bedload” in Figure 2d, and Figure 2i and Figure 2m) is
 164 characterized by a constant and relatively low sediment flux (i.e. similar to that imposed
 165 by the boundary conditions to the storage area, $35 < Q_s < 100$ g/s), and a coarse grain
 166 size distribution inherited from the coarser surface of the sediment deposit being the first
 167 to be destabilized (Piantini et al., 2021). This phase is dilute ($\phi \in [0.15: 0.25]$), exhibits
 168 typical bedload dynamics with grains saltating, rolling, and sliding on the bed (see movie

169 S1 and S2) with a mean downstream particle velocity $u_x \approx 0.27$ m/s (Figure 2e), and
 170 lasts for about 60 ± 30 seconds.

171 - Phase II (“Highly concentrated sediment flow” in Figure 2b-c, and Figure
 172 2i and Figure 2m) is characterized by a high sediment flux ($Q_s > 150$ g/s) exhibiting a
 173 wide grain size distribution made of a varying amount of fines ($D < 2$ mm). This phase
 174 corresponds to the maximum volume erosion in the sediment deposit causing a thick
 175 sediment flow ($\sim 3 - 3.5$ cm) with a downstream propagation that lasts for about $30 \pm$
 176 10 seconds (Piantini et al., 2021). The flow exhibits a strong vertical rheological
 177 stratification (see movie S1 and S2): surface particles are mainly driven by boundary
 178 shear stress (i.e. flowing water) and grain collisions, while deeper particles move slower
 179 likely as a result of frictional and enduring contacts between grains. A strong increase in
 180 fine content during phase II leads to further vertical heterogeneities in terms of grain sizes
 181 thanks to the occurrence of grain sorting processes (Frey & Church, 2009; Johnson et al.,
 182 2012), for which the biggest particles are pushed towards the surface (see movie S1 and
 183 movie S2). When the content of fines is low ($C_{D < 2 \text{ mm}}^{\text{Phase II}} < 10$ %), we estimate a mean
 184 downstream surface particle velocity of $u_x \approx 0.17$ m/s, while when the content is higher
 185 ($C_{D < 2 \text{ mm}}^{\text{Phase II}} > 35$ %) we have $u_x \approx 0.39$ m/s (Figure 2e). The average downstream
 186 velocity of the thick sediment flow is estimated to be much slower than surface particles
 187 ($U_x \approx 0.10$ m/s, Supporting Information). The volumetric solid concentration of phase II
 188 is highly variable in time ($\phi \in [0.30: 0.50]$), consistent with previous observations
 189 regarding debris flows (Iverson et al., 2010). The observed vertical stratification suggests
 190 an increasing volumetric solid concentration with depth, thus ϕ must be seen as depth-
 191 averaged. This behaviour appears as similar to observed for sheetflows on steep slopes
 192 (Palucis et al., 2018) and highly concentrated sediment flows (Armanini et al., 2005;
 193 Manville & White, 2003; Y. K. Sohn, 1997), where a flux of particles driven by shear
 194 stress overlays a denser sediment flow that moves *en masse*.

195 - Phase III %) (“Tail bedload” in Figure 2a, and Figure 2i and Figure 2m) is
 196 characterized by a low sediment flux ($35 < Q_s < 150$ g/s) and low values of volumetric
 197 solid concentration ($\phi \in [0.15: 0.25]$) similar to phase I. However, it exhibits a wider
 198 and finer grain size distribution ($C_{D > 8 \text{ mm}}^{\text{Phase I}} = 58\%$ against $C_{D > 8 \text{ mm}}^{\text{Phase III}} = 27$). This phase
 199 lasts for about 90 ± 15 seconds, and corresponds to the final stage of the erosion
 200 processes occurring in the sediment deposit. Phase III is characterized by a typical
 201 bedload dynamics (see movie S1 and S2) with a mean downstream particle velocity
 202 $u_x \approx 0.30$ m/s.

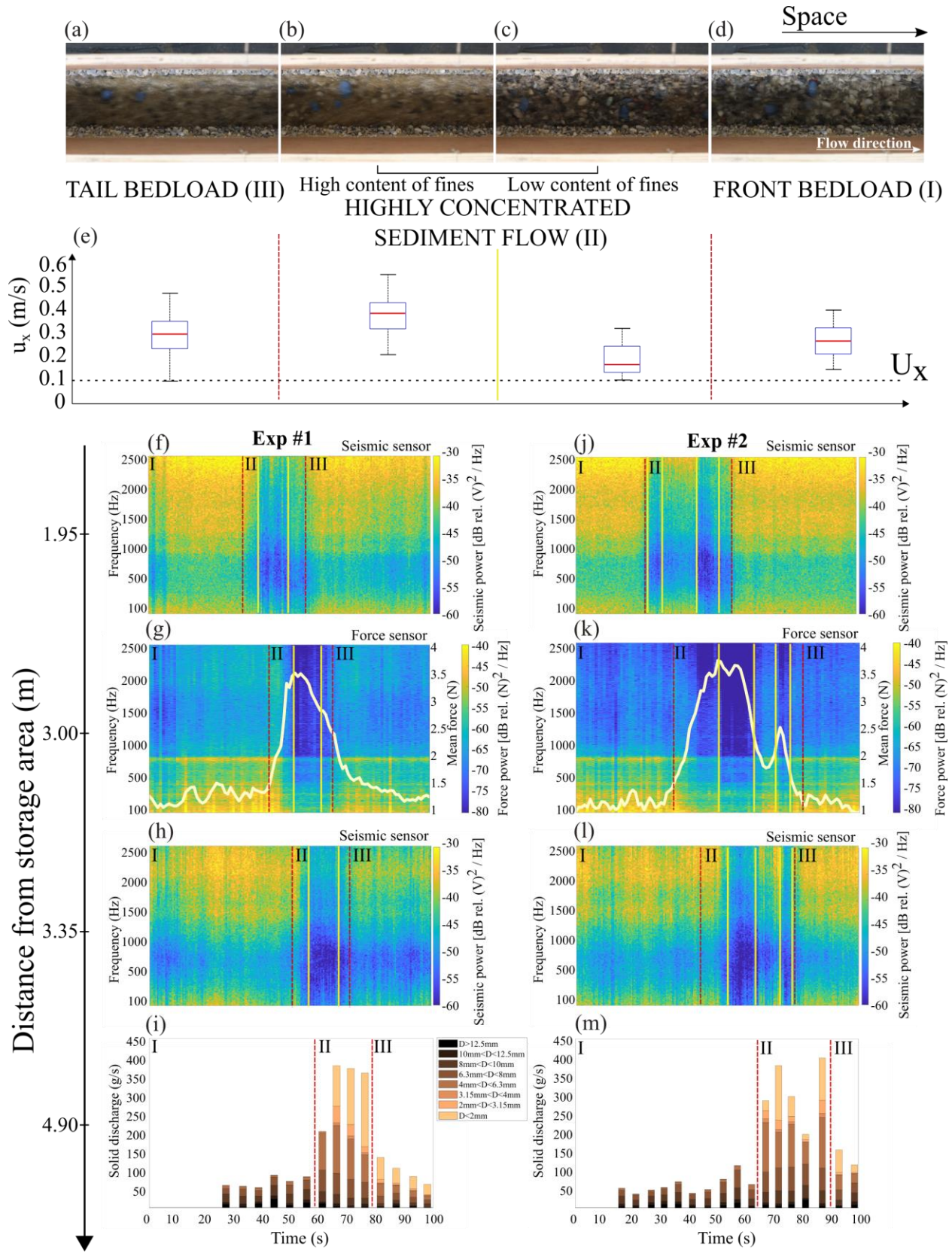
203 3.1.2 Force fluctuations and seismic observations

204 The three phases documented above have distinct seismic and force fluctuation
 205 signatures (Figure 2f-g-h and Figure 2j-k-l). Phases I and III generate the highest seismic
 206 and force power over the whole frequency range of interest. Phase I is associated with
 207 force power on average 3 dB higher than phase III likely as a result of differences in
 208 grain size distribution and downstream particle velocity, as expected from existing
 209 theories (Farin et al., 2019; Lai et al., 2018; Tsai et al., 2012) and as discussed further in
 210 section 4.1. The passage of the highly concentrated sediment flow (phase II, showed
 211 between vertical dashed red lines in Figure 2f-i and Figure 2j-m) is materialized by the
 212 sharp increase in mean basal force (i.e. sediment flow mass M , Figure 2g and Figure 2k).

213 Interestingly, it is associated with a strong reduction of on average about 10 dB in both
214 seismic and force power (Figure 2f-g-h and Figure 2j-k-l) compared to phase I and III.
215 We also find that the largest drops in force and seismic power always occur when the
216 maximum flux of fines passes through the sections closest to the respective seismic and
217 force sensors (see yellow squares in Figure 2f-g-h and Figure 2j-k-l). These observations
218 made using the camera are also confirmed by the time delay observed between the lowest
219 levels of force power and the outlet sediment flux measurements characterized by the
220 maximum content of fines, which is consistent with that predicted using the estimated
221 downstream velocity of the sediment flux. In order to better interpret the variations in

222 force power associated with the highly concentrated sediment flow, we push forward our
223 investigation by analysing the link between force power and flow bulk properties.

224



226 **Figure 2.** (a-d) Photos from the upstream camera showing the phases of a typical pulse; (e) Box
 227 plots for the downstream particle velocity for each phase. The bottom and top of each box are the
 228 25th and 75th percentiles of the sample, while the red line in the middle represents the median.
 229 The whiskers above and below each box go to the furthest observations. U_x is shown with the
 230 horizontal dotted line. (f-h) and (j-l) Seismic power detected by the upstream and downstream
 231 seismic sensor, respectively. It is shown as a function of time and frequency. Different colors
 232 refer to different levels of power. (g-k) Force power and mean force detected by the force sensor.
 233 (i-m) Outlet sediment flux measurements. Each colored bar refers to the particle diameter
 234 displayed in the legend, and the bar length is proportional to the percentage in weight of the
 235 related size. The vertical dashed red lines divide the three different phases presented in the
 236 photos above, while the yellow squares delimit the time interval with the maximum content of
 237 fines in phase II.

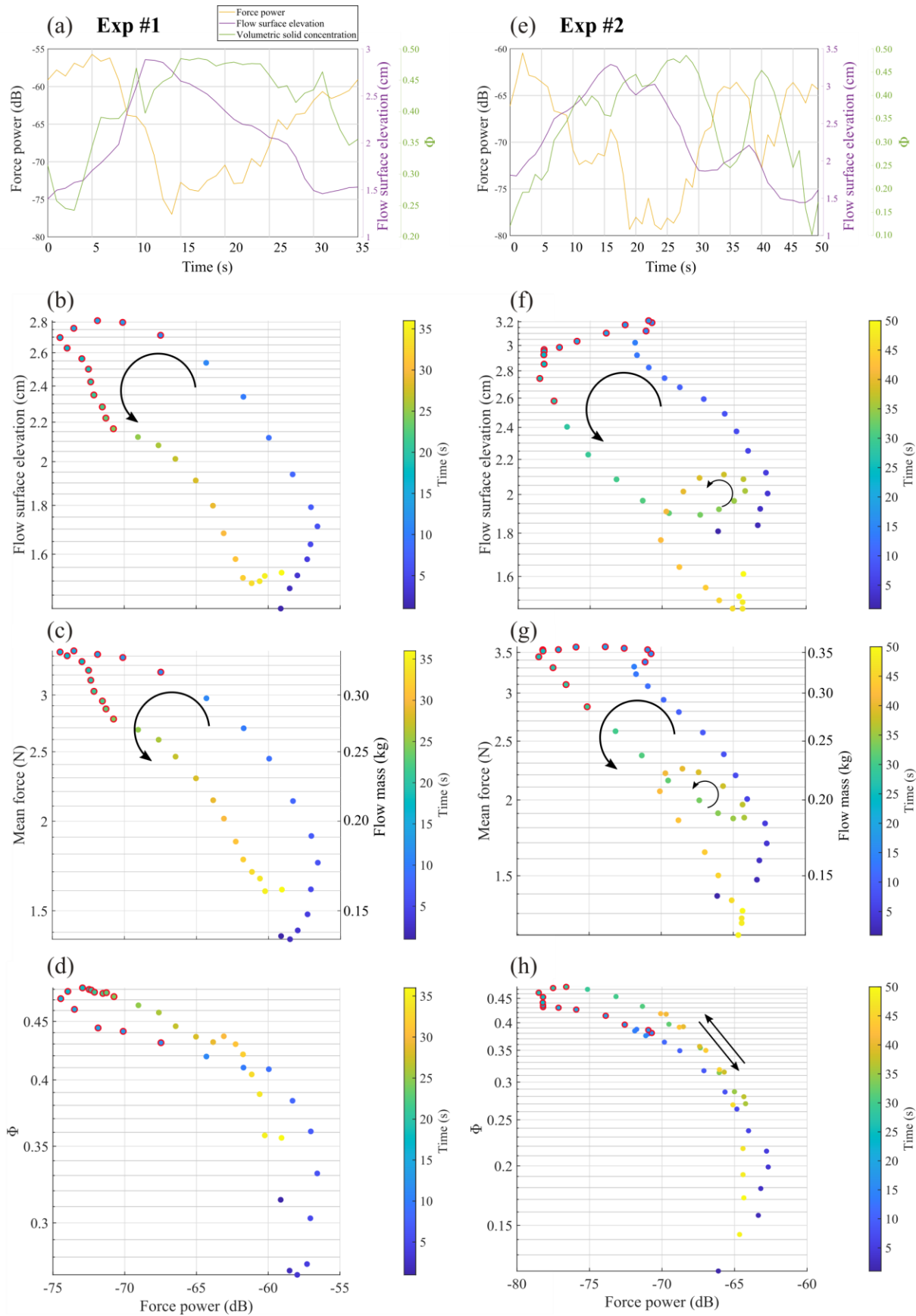
238

239 3.2 Linking force power with the properties of the highly concentrated sediment flows

240 In Figure 3 we express flow surface elevation (h), mean basal force (\bar{F}), and volumetric
 241 solid concentration (Φ) as a function of the measured force power. The very first seconds of the
 242 highly concentrated sediment flows are characterized by weak positive relationships between
 243 force power and h , \bar{F} , and Φ (Figure 3b-d and Figure 3f-h). However, at this stage of the
 244 experiment these measurements are quite uncertain as a result of being affected by local and
 245 transient grain depositions (Supporting Information). Past an inflexion point corresponding to
 246 $\Phi = 0.36$ for Exp #1 and $\Phi = 0.21$ for Exp #2, the relationship between force power and flow
 247 properties becomes negative. We observe large counter-clockwise hysteresis in the relationships
 248 between force power and h and \bar{F} : a given mean basal force and flow surface elevation is
 249 associated with significantly different values of force power (5 up to 10 dB differences). This
 250 hysteresis behaviour is due to force power decreasing and remaining low after peak h and \bar{F} are
 251 reached (Figure 2f and Figure 2j, and Figure 3a and Figure 3e). Interestingly, this hysteresis is no
 252 longer significantly observed when force power is evaluated versus Φ (Figure 3d and Figure
 253 3h), in which case maximum Φ always corresponds to minimum force power (Figure 3b and
 254 Figure 3f). Although a small clockwise hysteresis may be distinguished between force power and
 255 Φ for the presently considered examples, we do not consider it as significant because (i) it is not
 256 systematically observed for other sediment flows presented in the Supporting Information, where
 257 the rising and falling limbs of Φ collapse on a unique curve, and (ii) it becomes much less clear
 258 when reducing the moving average window size applied for smoothing the data, as opposed to
 259 versus h and \bar{F} (Supporting Information). Our finding of a direct link between force power and
 260 Φ is also supported by observations at shorter time scales. Indeed, we observe drastic changes in
 261 the relationship between force power and h and \bar{F} , materialized by a small loop around $t = 35$ s

262 in Exp #2 (Figure 3f-g) that are no longer visible in Figure 3h as a result of being associated with
263 according changes in Φ .

264



266 **Figure 3.** All panels refer to phase II. (a) and (e) show the evolution in time of the force power,
 267 h , and Φ . The log-log scatterplots of (b-c-d) and (f-g-h) show force power on the x axis and flow
 268 properties on the y axis. M is computed by multiplying the mean force by g . The time interval
 269 when the content of fines is maximum is marked in the scatterplots with red circles.

270

271 4 Discussion

272 4.1 Do existing theories explain our observations?

273 We find that the front bedload (phase I) is characterized by a slightly higher level of force
 274 power (+3 dB) than that of the tail bedload (phase III), both of which generate significantly
 275 higher force power levels (+10 dB) than that of the highly concentrated sediment flow (phase
 276 II). Sediment transport dynamics in phase I and III appears to be most consistent with that
 277 described in previous theories (Farin et al., 2019; Lai et al., 2018; Tsai et al., 2012), where force
 278 power is generated by the sum of individual particles impacting the bed at a rate and with a force
 279 that is mostly set by (i) the average downstream grain velocity, (ii) the grain size and (iii) the bed
 280 roughness. Particles constituting the front bedload move slower than those of the tail bedload
 281 ($u_x = 0.27$ m/s against $u_x = 0.30$ m/s), are associated with similar fluxes, but are on average
 282 coarser as the percentage of particles > 8 mm is double ($C_{D>8\text{mm}}^{\text{Phase I}} = 58\%$ and $C_{D>8\text{mm}}^{\text{Phase III}} =$
 283 27%). As a consequence, slightly larger grains likely explain the slightly higher force power of
 284 phase I, especially given the expected prevalence control of the larger grain fraction for our grain
 285 size distribution (Supporting Information).

286 Sediment transport dynamics as formulated in existing theories however cannot explain
 287 the force power associated with the highly concentrated sediment flow (phase II, Figure 3a and
 288 Figure 3c). During this phase, force power decreases abruptly by about -10 dB in less than 5
 289 seconds (Figure 3a and Figure 3c). Such a reduction is not associated with a decrease in sediment
 290 flux, which in fact increases, nor in a decrease of grain size, as the coarse fraction of the highly
 291 concentrated sediment is almost constant ($C_{D>8\text{mm}}^{\text{Phase II}} = 8\% \pm 2$ for Exp #1 and $C_{D>8\text{mm}}^{\text{Phase II}} =$
 292 $14\% \pm 2$ for Exp #2). We also exclude strong decreases in the averaged sediment flow velocity
 293 as a potential origin of this behaviour, since we do not observe spatial disconnections within
 294 phase II. As presented in section 3.1, particles at the surface are more agitated and move faster
 295 than underlying sediments. This is particularly evident when grain sorting occurs. Another
 296 possibility could be that these particles constitute the main source of force fluctuations as a result
 297 of being the biggest and the fastest, and that the thicker sediment flow beneath them dampens
 298 their contribution, resulting in lower force fluctuations on the bed as observed in the presence of
 299 static sediment deposits (Kean et al., 2015; McCoy et al., 2013). However, we do not find this
 300 process primarily explains our observations because: (i) when particles at the surface reach
 301 maximum velocity, force power in fact reaches its minimum (phase II with the presence of fines,
 302 Figure 2e) and (ii) there is not a unique link but a hysteresis between force power and the

303 thickness of the sediment flow (see hysteresis in Figure 3b and Figure 3f) as one would expect if
304 this latter controlled the attenuation of force fluctuations.

305 4.2 Volumetric solid concentration helps deciphering the force fluctuations generated by 306 the highly concentrated sediment flows

307 The key observation yielding further insight into the underlying source of reduced force
308 fluctuations of the highly concentrated sediment flow (phase II) is the negative relationship and
309 suppressed hysteresis behaviour between force power and volumetric solid concentration (Figure
310 3b and Figure 3f). Volumetric solid concentration is known to be a proxy for particle agitation
311 for dense granular flows, commonly described as granular temperature (Armanini et al., 2005;
312 Campbell, 1990; GDR MiDi, 2004; Iverson et al., 1997). Rapid and agitated granular flows are
313 characterized by low values of Φ as they dilate, while less agitated flows mean that particles
314 have poor capability to move past one other and tend to jam with slow long-lasting contacts,
315 leading to an increase in solid concentration (da Cruz et al., 2005; Forterre & Pouliquen, 2008).
316 Since particle agitation controls inter-particle collisions and impacts to the bed (Bachelet et al.,
317 2021; Farin et al., 2019), high values of solid concentration are associated with low force
318 fluctuations. The evolution of Φ over time may also explain the observed (i) presence of the
319 hysteresis and (ii) negative relationships between h and M and force power. Hysteresis may be
320 due to the percolation of fines in the voids within the coarse fraction of the mixture, which
321 optimizes the space occupied by particles and allows for an increase in Φ and thus a decrease in
322 the amplitude of force fluctuations regardless of h or M . Fines thus help dampening force
323 fluctuations primarily through increasing the Φ rather than pushing big particles far from the
324 bed, although this latter mechanism may still occur at a secondary level.

325 The finding of a negative relationship between force power and Φ is consistent with the
326 results of Allstadt et al. (2020), who highlight the existence of a negative correlation between the
327 normal fluctuating stresses and the bulk density of experimental debris flows. This finding could
328 appear in contradiction with Coviello et al. (2018) who show that a hyperconcentrated flow
329 generates higher seismic signals than more dilute sediment transport, however in their case the
330 coarse grain fraction also increase dramatically with sediment concentration. Past observations of
331 positive correlation in the relationships between h and M and force power as opposed to this
332 study (Allstadt et al., 2020; McCoy et al., 2013; Zhang, Walter, McArdeell, Haas, et al., 2021)
333 could also be explained in terms of Φ . Indeed, in the debris flows investigated by Allstadt et al.
334 (2020) and Zhang et al. (2021), bulk density decreases as h and M increase. Our interpretation
335 may be also consistent with the experiments of Hsu et al. (2014), who argue that the slightly
336 negative correlation observed between the force fluctuations and mean force for “the least
337 collisional” mud-saturated granular flow could be explained by a high ratio of solid to fluid
338 volume fraction. We therefore suggest that a positive relationship between force power and flow
339 surface elevation holds only when the latter is the result of dilation of the flow, causing enhanced
340 particle agitation. We acknowledge that this is often the case for natural debris flows (Iverson,
341 1997), although the extent it would apply to other sediment flows such as sheetflows or highly
342 concentrated sediment flows remains uncertain. Nevertheless, our present finding may provide a

343 path to unify these various flows into a single framework, in which the key requirement would
344 be to properly describe the dependency of volumetric solid concentration on flow characteristics.

345 4.3 Implications for theoretical models

346 Particle agitation controls the rate of impacts and impact velocities of particles of
347 sediment flows. In existing theoretical models, it is assumed to be a function of the average
348 downstream velocity of the flow (Bachelet et al., 2021; Farin et al., 2019; Zhang, Walter,
349 McArdell, Haas, et al., 2021), while volumetric solid concentration only comes into play through
350 controlling the number of particles impacting the bed (Farin et al., 2019; Zhang, Walter,
351 McArdell, Haas, et al., 2021). Here we propose that particle agitation should be incorporated as a
352 function of volumetric solid concentration or bulk density, equivalently (Jenkins & Askari,
353 1999). This would cause the link between force fluctuations and volumetric solid concentration
354 to be negative rather than positive, at least for sufficiently highly concentrated sediment flows.

355 5 Conclusions

356 We carry out laboratory experiments to explore the influence of grain scale processes in
357 the generation of force fluctuations of highly concentrated sediment flows. The key observation
358 yielding further insight onto the underlying source of force fluctuations is the clear negative
359 relationship between their amplitude and volumetric solid concentration. We interpret this result
360 by considering the volumetric solid concentration as a proxy for the degree of particle agitation.
361 Our present finding may also provide a path to unify various flows into a single framework, in
362 which the key requirement would be to properly describe the dependency of volumetric solid
363 concentration on flow characteristics.

364

365 Acknowledgments

366 The authors declare no conflict of interest. This research has been supported by the Agence
367 Nationale de la Recherche (grant no. 17-CE01-0008). We acknowledge the support of the
368 INRAE Research Centre of Grenoble for the laboratory and instrumental equipment. We thank
369 Jeroni Salens for helping in the development of the force plate and sensor, and Xavier Berti for
370 the fruitful scientific discussions.

371

372 Open Research

373 The data analysed during the current study are available on the Zenodo platform via

374 <https://doi.org/10.5281/zenodo.6761000>

375

376

377

378

379 **References**

- 380 Allstadt, K. E., Farin, M., Iverson, R. M., Obryk, M. K., Kean, J. W., Tsai, V. C., Rapstine, T.
381 D., & Logan, M. (2020). Measuring Basal Force Fluctuations of Debris Flows Using
382 Seismic Recordings and Empirical Green's Functions. *Journal of Geophysical Research:
383 Earth Surface*, 125(9). <https://doi.org/10.1029/2020JF005590>
- 384 Arattano, M., & Moia, F. (1999). Monitoring the propagation of a debris flow along a torrent.
385 *Hydrological Sciences Journal*, 44(5), 811–823.
386 <https://doi.org/10.1080/02626669909492275>
- 387 Armanini, A., Capart, H., Fraccarollo, L., & Larcher, M. (2005). Rheological stratification in
388 experimental free-surface flows of granular–liquid mixtures. *Journal of Fluid Mechanics*,
389 532, 269–319. <https://doi.org/10.1017/S0022112005004283>
- 390 Bachelet, V., Mangeney, A., Toussaint, R., DeRosny, J., Farin, M., & Hibert, C. (2021). *Acoustic
391 emissions of nearly steady and uniform granular flows: A proxy for flow dynamics and
392 velocity fluctuations*. <https://doi.org/10.48550/ARXIV.2101.04161>
- 393 Bakker, M., Gimbert, F., Geay, T., Misset, C., Zanker, S., & Recking, A. (2020). Field
394 Application and Validation of a Seismic Bedload Transport Model. *Journal of
395 Geophysical Research: Earth Surface*, 125(5). <https://doi.org/10.1029/2019JF005416>
- 396 Burtin, A., Hovius, N., & Turowski, J. M. (2016). Seismic monitoring of torrential and fluvial
397 processes. *Earth Surface Dynamics*, 4(2), 285–307. [https://doi.org/10.5194/esurf-4-285-
398 2016](https://doi.org/10.5194/esurf-4-285-2016)
- 399 Campbell, C. S. (1990). *Rapid Granular Flows*. 36.

- 400 Casagli, N., Ermini, L., & Rosati, G. (2003). Determining grain size distribution of the material
401 composing landslide dams in the Northern Apennines: Sampling and processing methods.
402 *Engineering Geology*, 69(1–2), 83–97. [https://doi.org/10.1016/S0013-7952\(02\)00249-1](https://doi.org/10.1016/S0013-7952(02)00249-1)
- 403 Cole, S. E., Cronin, S. J., Sherburn, S., & Manville, V. (2009). Seismic signals of snow-slurry
404 lahars in motion: 25 September 2007, Mt Ruapehu, New Zealand. *Geophysical Research*
405 *Letters*, 36(9), L09405. <https://doi.org/10.1029/2009GL038030>
- 406 Cook, K. L., Andermann, C., Gimbert, F., Adhikari, B. R., & Hovius, N. (2018). Glacial lake
407 outburst floods as drivers of fluvial erosion in the Himalaya. *Science*, 362(6410), 53–57.
408 <https://doi.org/10.1126/science.aat4981>
- 409 Cook, K. L., Rekapalli, R., Dietze, M., Pilz, M., Cesca, S., Rao, N. P., Srinagesh, D., Paul, H.,
410 Metz, M., Mandal, P., Suresh, G., Cotton, F., Tiwari, V. M., & Hovius, N. (2021).
411 Detection and potential early warning of catastrophic flow events with regional seismic
412 networks. *Science*, 374(6563), 87–92. <https://doi.org/10.1126/science.abj1227>
- 413 Coviello, V., Arattano, M., Comiti, F., Macconi, P., & Marchi, L. (2019). Seismic
414 Characterization of Debris Flows: Insights into Energy Radiation and Implications for
415 Warning. *Journal of Geophysical Research: Earth Surface*, 124(6), 1440–1463.
416 <https://doi.org/10.1029/2018JF004683>
- 417 Coviello, V., Capra, L., Vázquez, R., & Márquez-Ramírez, V. H. (2018). Seismic
418 characterization of hyperconcentrated flows in a volcanic environment: Seismic
419 characterization of hyperconcentrated flows. *Earth Surface Processes and Landforms*,
420 43(10), 2219–2231. <https://doi.org/10.1002/esp.4387>

- 421 da Cruz, F., Emam, S., Prochnow, M., Roux, J.-N., & Chevoir, F. (2005). Rheophysics of dense
422 granular materials: Discrete simulation of plane shear flows. *Physical Review E*, *72*(2),
423 021309. <https://doi.org/10.1103/PhysRevE.72.021309>
- 424 Farin, M., Tsai, V. C., Lamb, M. P., & Allstadt, K. E. (2019). A physical model of the high-
425 frequency seismic signal generated by debris flows. *Earth Surface Processes and*
426 *Landforms*, *44*(13), 2529–2543. <https://doi.org/10.1002/esp.4677>
- 427 Forterre, Y., & Pouliquen, O. (2008). Flows of Dense Granular Media. *Annual Review of Fluid*
428 *Mechanics*, *40*(1), 1–24. <https://doi.org/10.1146/annurev.fluid.40.111406.102142>
- 429 Frey, P., & Church, M. (2009). How River Beds Move. *Science*, *325*(5947), 1509–1510.
430 <https://doi.org/10.1126/science.1178516>
- 431 GDR MiDi. (2004). On dense granular flows. *The European Physical Journal E*, *14*(4), 341–
432 365. <https://doi.org/10.1140/epje/i2003-10153-0>
- 433 Gimbert, F., Fuller, B. M., Lamb, M. P., Tsai, V. C., & Johnson, J. P. L. (2019). Particle
434 transport mechanics and induced seismic noise in steep flume experiments with
435 accelerometer-embedded tracers: Experimental Testing of Seismic Noise Generated by
436 Sediment Transport. *Earth Surface Processes and Landforms*, *44*(1), 219–241.
437 <https://doi.org/10.1002/esp.4495>
- 438 Govi, M., Maraga, F., & Moia, F. (1993). Seismic detectors for continuous bed load monitoring
439 in a gravel stream. *Hydrological Sciences Journal*, *38*(2), 123–132.
440 <https://doi.org/10.1080/02626669309492650>
- 441 Haas, T., Åberg, A. S., Walter, F., & Zhang, Z. (2021). Deciphering seismic and normal-force
442 fluctuation signatures of debris flows: An experimental assessment of effects of flow

- 443 composition and dynamics. *Earth Surface Processes and Landforms*, esp.5168.
444 <https://doi.org/10.1002/esp.5168>
- 445 Hsu, L., Dietrich, W. E., & Sklar, L. S. (2014). Mean and fluctuating basal forces generated by
446 granular flows: Laboratory observations in a large vertically rotating drum. *Journal of*
447 *Geophysical Research: Earth Surface*, 119(6), 1283–1309.
448 <https://doi.org/10.1002/2013JF003078>
- 449 Iverson, R. M. (1997). The physics of debris flows. *Reviews of Geophysics*, 35(3), 245–296.
450 <https://doi.org/10.1029/97RG00426>
- 451 Iverson, R. M., Logan, M., LaHusen, R. G., & Berti, M. (2010). The perfect debris flow?
452 Aggregated results from 28 large-scale experiments. *Journal of Geophysical Research*,
453 115(F3), F03005. <https://doi.org/10.1029/2009JF001514>
- 454 Iverson, R. M., Reid, M. E., & LaHusen, R. G. (1997). Debris-flow mobilization from landslides.
455 *Annual Review of Earth and Planetary Sciences*, 25(1), 85–138.
456 <https://doi.org/10.1146/annurev.earth.25.1.85>
- 457 Jenkins, J. T., & Askari, E. (1999). *Hydraulic theory for a debris flow supported on a collisional*
458 *shear layer*. 9(3), 6.
- 459 John Wolcott. (1988). Nonfluvial Control of Bimodal Grain-Size Distributions in River-Bed
460 Gravels. *SEPM Journal of Sedimentary Research*, Vol. 58.
461 <https://doi.org/10.1306/212F8ED6-2B24-11D7-8648000102C1865D>
- 462 Johnson, C. G., Kokelaar, B. P., Iverson, R. M., Logan, M., LaHusen, R. G., & Gray, J. M. N. T.
463 (2012). Grain-size segregation and levee formation in geophysical mass flows: LEVEE
464 FORMATION IN GEOPHYSICAL FLOWS. *Journal of Geophysical Research: Earth*
465 *Surface*, 117(F1), n/a-n/a. <https://doi.org/10.1029/2011JF002185>

- 466 Kean, J. W., Coe, J. A., Coviello, V., Smith, J. B., McCoy, S. W., & Arattano, M. (2015).
467 Estimating rates of debris flow entrainment from ground vibrations: GROUND
468 VIBRATIONS FROM DEBRIS FLOWS. *Geophysical Research Letters*, *42*(15), 6365–
469 6372. <https://doi.org/10.1002/2015GL064811>
- 470 Lagarde, S., Dietze, M., Gimbert, F., Laronne, J. B., Turowski, J. M., & Halfi, E. (2021). Grain-
471 Size Distribution and Propagation Effects on Seismic Signals Generated by Bedload
472 Transport. *Water Resources Research*, *57*(4). <https://doi.org/10.1029/2020WR028700>
- 473 Lai, V. H., Tsai, V. C., Lamb, M. P., Ulizio, T. P., & Beer, A. R. (2018). The Seismic Signature
474 of Debris Flows: Flow Mechanics and Early Warning at Montecito, California.
475 *Geophysical Research Letters*, *45*(11), 5528–5535.
476 <https://doi.org/10.1029/2018GL077683>
- 477 Larose, E., Carrière, S., Voisin, C., Bottelin, P., Baillet, L., Guéguen, P., Walter, F., Jongmans,
478 D., Guillier, B., Garambois, S., Gimbert, F., & Massey, C. (2015). Environmental
479 seismology: What can we learn on earth surface processes with ambient noise? *Journal of*
480 *Applied Geophysics*, *116*, 62–74. <https://doi.org/10.1016/j.jappgeo.2015.02.001>
- 481 Manville, V., & White, J. D. L. (2003). Incipient granular mass flows at the base of sediment-
482 laden floods, and the roles of flow competence and flow capacity in the deposition of
483 stratified bouldery sands. *Sedimentary Geology*, *155*(1–2), 157–173.
484 [https://doi.org/10.1016/S0037-0738\(02\)00294-4](https://doi.org/10.1016/S0037-0738(02)00294-4)
- 485 McCoy, S. W., Tucker, G. E., Kean, J. W., & Coe, J. A. (2013). Field measurement of basal
486 forces generated by erosive debris flows: DEBRIS FLOW BASAL FORCE. *Journal of*
487 *Geophysical Research: Earth Surface*, *118*(2), 589–602.
488 <https://doi.org/10.1002/jgrf.20041>

- 489 Palucis, M. C., Ulizio, T., Fuller, B., & Lamb, M. P. (2018). Intense Granular Sheetflow in Steep
490 Streams. *Geophysical Research Letters*, 45(11), 5509–5517.
491 <https://doi.org/10.1029/2018GL077526>
- 492 Piantini, M., Gimbert, F., Bellot, H., & Recking, A. (2021). Triggering and propagation of
493 exogenous sediment pulses in mountain channels: Insights from flume experiments with
494 seismic monitoring. *Earth Surface Dynamics*, 9(6), 1423–1439.
495 <https://doi.org/10.5194/esurf-9-1423-2021>
- 496 Roth, D. L., Brodsky, E. E., Finnegan, N. J., Rickenmann, Dieter., Turowski, J. M., & Badoux,
497 A. (2016). Bed load sediment transport inferred from seismic signals near a river. *Journal*
498 *of Geophysical Research: Earth Surface*, 121(4), 725–747.
499 <https://doi.org/10.1002/2015JF003782>
- 500 Sklar, L. S., Riebe, C. S., Marshall, J. A., Genetti, J., Leclere, S., Lukens, C. L., & Mercedes, V.
501 (2017). The problem of predicting the size distribution of sediment supplied by hillslopes
502 to rivers. *Geomorphology*, 277, 31–49. <https://doi.org/10.1016/j.geomorph.2016.05.005>
- 503 Tsai, V. C., Minchew, B., Lamb, M. P., & Ampuero, J.-P. (2012). A physical model for seismic
504 noise generation from sediment transport in rivers: SEISMIC NOISE FROM
505 SEDIMENT TRANSPORT. *Geophysical Research Letters*, 39(2), n/a-n/a.
506 <https://doi.org/10.1029/2011GL050255>
- 507 Welch, P. (1967). The use of fast Fourier transform for the estimation of power spectra: A
508 method based on time averaging over short, modified periodograms. *IEEE Transactions*
509 *on Audio and Electroacoustics*, 15(2), 70–73. <https://doi.org/10.1109/TAU.1967.1161901>
- 510 Y. K. Sohn. (1997). On Traction-Carpet Sedimentation. *SEPM Journal of Sedimentary Research*,
511 *Vol. 67*. <https://doi.org/10.1306/D42685AE-2B26-11D7-8648000102C1865D>

512 Zhang, Z., Walter, F., McArdell, B. W., Haas, T., Wenner, M., Chmiel, M., & He, S. (2021).

513 Analyzing Bulk Flow Characteristics of Debris Flows Using Their High Frequency

514 Seismic Signature. *Journal of Geophysical Research: Solid Earth*, 126(12).

515 <https://doi.org/10.1029/2021JB022755>

516 Zhang, Z., Walter, F., McArdell, B. W., Wenner, M., Chmiel, M., de Haas, T., & He, S. (2021).

517 Insights From the Particle Impact Model Into the High-Frequency Seismic Signature of

518 Debris Flows. *Geophysical Research Letters*, 48(1).

519 <https://doi.org/10.1029/2020GL088994>

520

521